Infrared Delamination Defect Detection of Type III Aluminium Lined Gas Cylinder

Yuanhui ZHANG [1], Chunqiao YU [2]*, Jie ZHANG [2, 3], Ting ZHENG [1], Bin WANG [3]

[1] *College of Intelligent Manufacturing and Automotive Engineering, Luzhou Vocational and Technical College, Luzhou Sichuan 646000*
[2] *School of Mechatronic Engineering, Southwest Petroleum University, Chengdu Sichuan 610500*
[3] *School of New Energy and Materials, Southwest Petroleum University, Chengdu Sichuan 610500*

http://doi.org/10.5755/j02.ms.42862

Received 24 September 2025; accepted 2 December 2025

In this study, the influence of two thermal loading methods, internal excitation and external excitation, on the defect detection effect is systematically investigated for the difficult problem of detecting delamination defects in carbon fibre-wound gas cylinders with the aluminium inner liner of type III. By establishing an axisymmetric two-dimensional model of the gas cylinder, the heat conduction process under different defect parameters (length, thickness, and depth) was simulated, and the multi-parameter coupling effect was analysed by using orthogonal tests. The results show that the external thermal excitation method is significantly better than the internal excitation in terms of detection sensitivity, temperature difference contrast and time resolution, and the optimal detection time window is 45 – 90 seconds. The peak thermal image temperature difference increases approximately linearly with the defect length, and its growth rate increases with the defect thickness and tends to stabilise, and the defect depth increases, resulting in a gradual decrease in the peak thermal image temperature difference and a slower decrease in the magnitude of the peak temperature difference; on the analysis of the significance of the defect parameters, the depth of the defects has the most significant effect on the temperature difference (contribution rate of 53.7 %), followed by the length of the defects (contribution rate of 19.2 %), and the defect thickness has a smaller effect (contribution rate of 6.5 %). This study provides a theoretical basis and optimisation scheme for the non-destructive testing of delamination defects in type III gas cylinders.
Keywords: composite gas cylinders, infrared thermography, delamination defects, orthogonal tests, non-destructive testing.

1. INTRODUCTION

Composite pressure vessels are widely used in petroleum, chemical, and ocean engineering fields because of their lightweight, high strength, and corrosion resistance. Composite fibre wrapping around metal liners can optimize their mechanical properties and achieve high durability and reliability [1 – 3]. For example, in the field of oil and gas, composite cylinders replace traditional metal cylinders to solve the problem of corrosion under the sea or in highly corrosive environments, and extend the service life. In hydrogen energy storage and transport, composite materials are mainly used as a protective shell to resist internal loads, preventing hydrogen embrittlement phenomenon and enhancing safety [4 – 8], so that the hydrogen storage cylinders have a higher strength and excellent sealing properties. Composite cylinders are susceptible to different types of damage in harsh operating environments. Ensuring the safety and integrity of composite structures has become an urgent issue, and therefore, regular non-destructive testing of composite cylinders is required. Defects in composite gas cylinders may come from the manufacturing of the material, the production, or the use process. Simple visual inspection can observe macroscopic defects during the manufacturing and installation of the cylinder, as well as during operation, such as surface cracks, scratches, leaks, etc. Internal defects in cylinders, such as delamination, matrix cracking, and interfacial debonding, require the use of non-destructive testing (NDT) techniques to assess the structural integrity of the cylinder without compromising its functionality [9 – 11]. Several techniques have been developed over the years, including ultrasonic scanning, radiography, thermography, and visual inspection [12]. These techniques utilise physical principles to determine the properties of a material or system. The primary goal is to identify and assess irregularities and harmful defects without compromising the integrity of the material, component or system. Infrared thermography is widely used in a variety of work scenarios due to its small cost and high efficiency, and the use of infrared thermography to quantitatively identify internal defects in composites is an important development direction for non-destructive testing technology [13]. Infrared thermography can be operated in bilateral or unilateral access mode, and various heat sources, including flash lamps, lasers, and ultrasonic vibration, can be used in these applications. Thermal excitation is applied to the gas cylinder to be tested, and heat is transferred in the cylinder, and the defects, due to the difference with the cylinder material, can be shown in the thermal image on the surface of the cylinder [14, 15]. Al-Athel et al [16] proposed a hybrid method that combines thermography, computational simulation, and an artificial neural network

* Corresponding author: C. Yu
E-mail: *202421000376@stu.swpu.edu.cn*

(ANN) hybrid method for detecting subsurface defects in composites. The ANN was trained by simulating thermography experimentally generated data to predict the depth of defects in plates and pipes with an accuracy of 10% and 19 %, respectively. The method does not rely on experimental data and can directly predict the shape and size of the damage. Ekanayake et al. [17] designed a method based on phase-locked thermography for accurately measuring the depth information of defects in CFRP structures, focusing on analysing the effects of lateral heat flow and contact resistance on the measurement accuracy. The method was shown to be capable of accurately determining the depth over a wide range of thicknesses and blind hole diameters with deviations less than 0.5 mm. Daghigh and Naraghi [18]used infrared thermography (IRT) combined with the k-nearest neighbour (k-NN) machine learning algorithm (ML) to solve the inverse heat transfer problem for defect detection in composites. Based on 502 sets of data generated by ABAQUS finite element simulation, surface temperature spatial and temporal features were extracted to train the model, and the trained ML could eventually predict the defect size, depth and thickness. Marcella Grosso et al. [19] simulated the model by active pulsed thermography, and investigated the effect of annulus thickness, heating time, and excitation energy on the detection limit of defects in composite joints, and the pulsed thermography could detect the defects in such composite joints. The technique was able to detect glue defects at a depth of 8.5 mm in this composite joint. Adisorn Sirikham et al. [20] used pulsed thermography to reconstruct visual defects in the form of 3D images of semi-closed air-gap composite specimens and steel specimens to validate the feasibility and effectiveness of the method, which provided relatively low mean percentage error for composite specimens, and estimated the total 3D defect volume to be less than 0.5 mm, estimating the total 3D defect volume to be less than 10 %. V Kalyanavalli et al. [21] long-pulse thermography for the determination of defect depth in basalt fibre-reinforced epoxy composites was carried out. Flat-bottomed holes with specific depth and size were fabricated in the composites to simulate delamination defects. The thermal contrast of the thermograms and the characteristic peak time were studied to obtain the slope-peak time of the long-pulse thermograms with respect to the depth of defects. The relationship between the slope peak time of long pulse thermography and the depth of defects is obtained. This paper establishes a model of hydrogen storage cylinder with delamination defects in type III composite material, compares the detection effect of internal and external excitation methods on the cylinder, analyses the influence of delamination defect parameters on the temperature difference detection of the cylinder, and the results of the research can provide theoretical basis for the application of defect detection technology and safety evaluation of the cylinder.

2. FINITE ELEMENT ANALYSIS

2.1. Geometric modelling

Since the overall structure of the type III bottle presents axisymmetric geometric characteristics, the longitudinal section of the aluminium lining layer and the carbon fibre winding layer of the type III bottle is selected as the modelling reference to improve the modelling efficiency. For the interlayer defects of the carbon fibre winding layer, the delamination defects are set in the form of embedded defect sheets, and the shape of the defects is rectangular[22]. Using finite element software, the 2D plane model of the delamination defects of the type III bottle is established and meshed, and the geometric parameters are shown in Fig. 1.

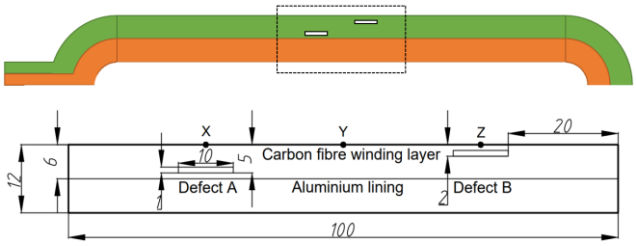

Fig. 1. Specimen model of delamination defects of the type III bottle

In this case, in order to simulate the material tear damage that often occurs in carbon fibre material cylinders, the delamination defects are air, and the parameters of the rest of the materials are shown in Table 1 [23].

Table 1. Thermophysical properties of type III cylinder materials

Material	Density, $kg \cdot m^{-3}$	Specific heat, $J \cdot (kg \cdot K)^{-1}$	Thermal conductivity, $W \cdot (m \cdot K)^{-1}$
Aluminium lining	2719	902	167
Carbon fibre	1570	840	0.7
Air	1.12	1017	0.022

2.2. Loading parameter settings

Currently, the main methods of heat source loading for Type III cylinders include internal excitation and external excitation. Internal excitation uses methods such as hot water injection and drainage or steam injection, while external excitation uses heating lamps to heat the surface of the cylinder. In order to compare the differences in detection effects between the two excitation methods, this study conducted separate simulation analyses.

2.2.1. Internal excitation simulation

Inside the gas cylinder, 80 ℃ constant temperature hot water was used as the continuous thermal excitation source, the thermal loading time was 150 seconds, and the simulation time step was set to 5 seconds. The thermal excitation is applied to the inner surface of the aluminium lining layer, and the outer wall of the cylinder is set to be at an ambient temperature of 25 ℃. The upper boundary of the model adopts natural convection boundary conditions. Natural convection boundary conditions were adopted at the upper boundary of the model, focusing on the observation of the transient heat transfer process in the time range of 0 – 80 s. The temperature field distribution data on the surface of the gas cylinder were recorded at the characteristic time points of 10 s, 30 s, 60 s, 100 s and 150 s. The simulation results in Fig. 2 show that the temperature in the deep defect region is significantly lower than that in the shallow defect region, and the surface temperature of the

carbon fibre layer containing defects is significantly lower than that in the defect-free region. This phenomenon originates from the low thermal conductivity property of the air defects, which leads to the blockage of heat flow transfer and thus reduces the heat conduction to the surface of the carbon fibre winding layer.

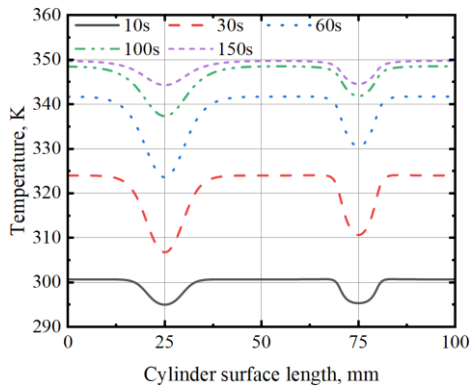

Fig. 2. Isothermal plot of heat flow excitation inside the cylinder

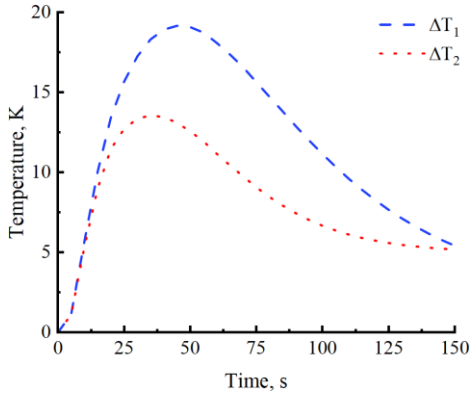

Fig. 3. Temperature difference versus excitation time under hot water excitation inside the cylinder

In order to quantitatively analyse the temperature distribution characteristics on the surface of the gas cylinder model, three characteristic monitoring points are selected on the surface of the model for comparative analysis: X(25,12) is located in the defective region, Y(50,12) is a defect-free reference point, and Z(75,12) is located in another defective region, and the position distribution is shown in Fig. 1. And remember ΔT_1 as the temperature difference between point X and point Y, $\Delta T_1=|T_X-T_Y|$, characterising the temperature difference in the defective region at point X; and remember ΔT_2 as the temperature difference between point Z and point Y, $\Delta T_2=|T_Z-T_Y|$, characterising the temperature difference in the defective region at point Z. The dynamic response curves of the two sets of temperature difference parameters ΔT_1 and ΔT_2 with respect to the excitation time are obtained through data processing, as shown in Fig. 3.

The results of the temperature response curves are shown in Fig. 3. Under the condition of a constant heat source, the temperature difference parameters ΔT_1 and ΔT_2 show obvious time-dependent characteristics. At the beginning of the excitation, both of them show a monotonous increasing tendency with the excitation time, and the growth rate of ΔT_1 is the highest at 0.91 K/s and that of ΔT_2 is 0.84 K/s. After reaching a critical point in time, around 45 s, continuous heating suppresses the effectiveness of the defects in blocking heat flow to the surface. This suppression causes a sharp decline in the ΔT_1 and ΔT_2 change rates. Given the closer proximity of defect B to the surface, ΔT_2 stabilizes faster than ΔT_1. The temperature difference curves tend to be stabilised, and the rate of change decreases significantly. For the delamination defect A, ΔT_1 reaches a peak value of 19.2 K at t = 45 s, as shown in Fig. 4 a, and then gradually decreases with a decay rate of 16 – 18 %, while the corresponding ΔT_2 reaches a stable state earlier than ΔT_1 at t = 35 s, with a peak value of 13.6 K, and then decreases with a decay rate of 12 – 15 % until the temperature difference stabilises. The optimal detection time window is 45 – 80 s, during which $\Delta T_1-\Delta T_2\geq 6$ K, the absolute value of the temperature difference is relatively stable, and the maximum value of 6.94 K is achieved at t = 65 s, with a significant temperature gradient distribution.

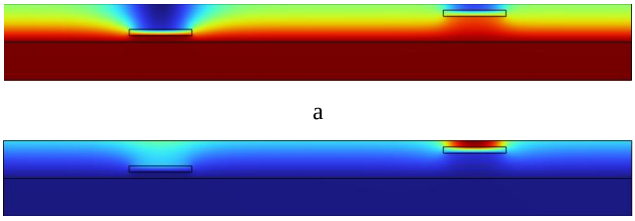

Fig. 4. Cloud view of peak temperature difference obtained by two excitation methods: a – plot of the peak temperature difference obtained by the excitation method in t = 45 s; b – plot of peak temperature difference obtained by t = 60 s external excitation mode

2.2.2. External excitation simulation

In the external thermal excitation simulation configuration, a constant heat flow density (3000 W/m²) is used as the external excitation source, which acts directly on the surface of the carbon fibre winding layer of the gas cylinder, while keeping the aluminium lining layer in the state of natural convection heat transfer, and the ambient temperature is 25 °C. The transient thermal response was continuously monitored for 150 s. The analysis of the external heat flow excitation data in Fig. 5 shows that under the external heat flow excitation condition, the surface temperature field of the carbon fibre winding layer shows a significant non-uniform distribution, the isotherms of the delamination defect region show an obvious convex pattern, and the surface temperature of the defect corresponds to the defect-free region is higher than that of the defect-free region, with a maximum of 35 K. The heat flow is transferred to the internal interface of defects and finally to the aluminium liner through the carbon fibre winding layer, and then to the internal interface of defects and finally to the aluminium liner. The heat flow through the carbon fibre winding layer is transferred to the defect interface inside the gas cylinder, and finally reaches the aluminium lining layer, which forms a local high temperature zone with a length of 4 – 8 mm due to the restriction of transverse heat diffusion and axial heat stacking effect caused by the thermal resistance of the defect area, and the phenomenon verifies that the external thermal excitation enhances the detection of delamination defects, and provides a clear basis of the

temperature field characteristics for the localization of the defects.

Follow the coordinates X (25,12), Y (50,12), Z (75,12) of the internal excitation experiment for temperature data acquisition. Define the temperature difference parameters under external excitation conditions, $\Delta T_1' = |T_X - T_Y|$, $\Delta T_2' = |T_Z - T_Y|$, to obtain the temperature difference data plots under the excitation of the external heat source of the cylinders, and the experimental data Fig. 6 shows that: in the initial heating stage (t < 30 s), both temperature difference curves show an approximate linear growth, $\Delta T_2'$ growth rate of 1.18 K/s was significantly higher than that of $\Delta T_1'$ of 0.15 K/s. $\Delta T_1'$ reached the maximum value of 7.9 K at t = 75 s, and $\Delta T_2'$ reached the peak value of 37.2 K at t = 60 s, as shown in Fig. 4 b, $\Delta T_2'$ is about 4.7 times higher than that of $\Delta T_1'$, $\Delta T_2'$ exhibits faster thermal response characteristics, with the peak appearing 15 s earlier, and the difference in steady-state temperature difference values is 29.3 K. This result confirms that the external thermal excitation method produces a more significant temperature contrast, which is conducive to the detection and identification of deep defects.

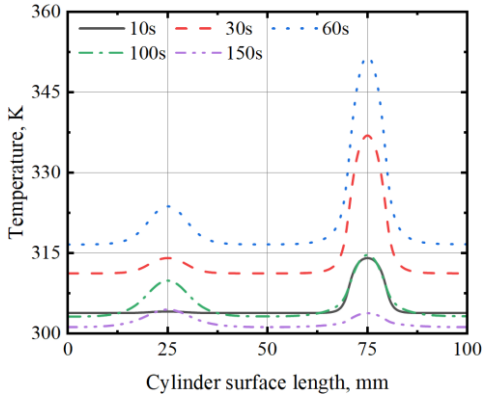

Fig. 5. Isothermal plot of heat flow excitation outside the cylinder

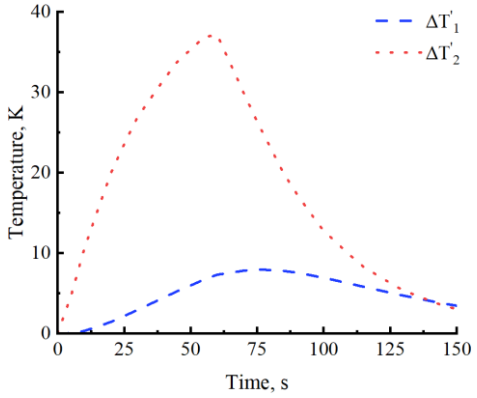

Fig. 6. Temperature difference versus excitation time under hot water excitation outside the cylinder

Through the comparative study of the two thermal loading modes of internal excitation of hot water circulation and external excitation of radiant heating, there are obvious differences in their dynamic response characteristics, the growth rate of temperature difference in the early stage of external excitation reaches 1.18 K/s, which is 1.3 times of that of the internal excitation of 0.91 K/s; the ratio of the maximal difference between the two excitation modes reaches 1.93:1, and the maximal difference of temperature generated by external excitation is 37.16 K, which is significantly higher than that of internal excitation of 19.17 K; the effective detection window is widened by 80 %, in the external excitation mode, the maximum difference between the two temperature differences between 45 – 90 s is 30.18 K, while the internal mode is only 6.94 K in 35 – 60 s; the external excitation enhances the temperature contrast at the edge of defects through the thermal resistance effect, the internal excitation is affected by the convective flow of fluids leading to the homogenisation of the temperature field, and the external excitation's radial heat flow is more conducive to the delamination of the defects are revealed. The experimental data confirm that the external radial heating method has significant advantages in terms of detection sensitivity, time resolution Δt = 5 s and defect visualisation, and is a better choice for the detection of delamination defects in type III gas cylinders. The conclusion provides a theoretical basis for the selection of NDT programmes in engineering practice.

3. ANALYSIS OF DEFECT PARAMETERS

The external thermal excitation method was chosen as the excitation method for the cylinders, keeping the same boundary conditions as in the previous experiments. To systematically study the influence of the geometric parameters of the defects, a univariate controlled experimental scheme was designed: the length *a* (2 – 10 mm), the thickness *b* (0.25 – 1.25 mm), and the depth *c* (0.5 – 4.5 mm) of the defects were respectively investigated by controlled-variable simulation, and only one parameter was changed in each experiment, and the rest of the parameters were fixed, so as to compare the influences of the different parameters on the value of the temperature difference of the thermal image, as shown in Fig. 7. Three characteristic monitoring points were set on the surface of the cylinder specimen, namely A (5,12), C (45,12), the defect-free point on the surface of the cylinder, and B (25,12) the delamination defect corresponding to the centre point of the cylinder surface. The average value of the temperatures at the two points A and C is taken as the temperature at the defect-free point, and ΔT is recorded as the absolute value of the temperature at the defect centre point and the corresponding point of the defect-free point on the surface of the winding layer, and $\Delta T = |T_B - (T_A + T_C)/2|$. This scheme can accurately quantify the defect geometrical parameters as a function of the surface temperature difference and establish a defect size-temperature difference correlation model, and through this strict univariate control method, it can effectively isolate the influence mechanism of each parameter on the thermal response.

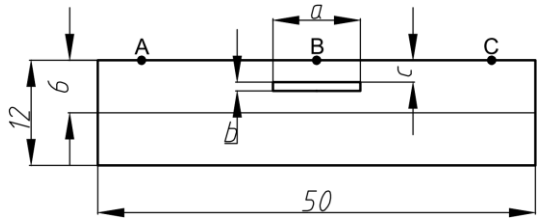

Fig. 7. Parametric model of delamination defects in type III bottles

3.1. Effect of defect length on heat transfer

Under the condition of fixed defect thickness b = 0.75 mm and depth c = 2.5 mm, a series of experiments are carried out by changing the defect length a (2 – 10 mm), and the response relationship between the defect length and the temperature difference is obtained as shown in Fig. 8. In the initial stage of 0 – 30 s, the temperature difference of all the specimens grows non-linearly, and the growth rate is positively correlated with the defect length, and the initial slope for the 10 mm defect is maximal at 0.3 K/s. The peak temperature difference $\Delta T_{\text{-peak}}$ is linearly related to the defect length, and a quantitative model of defect length-peak temperature difference is established, $\Delta T_{\text{-peak}} = k \cdot a + C$, where k = 1.53 and C = 1.21 scale factor verification: when a increases from 2 mm to 10 mm, $\Delta T_{\text{-peak}}$ grows 7.62 times with the theoretical prediction of a deviation of 0.56 %, and the experimental data confirms that, at a given thickness and depth, the defect length is the most important factor affecting the surface. The experimental data confirm that the defect length is a significant parameter affecting the surface temperature difference under the given thickness and depth conditions, and this finding provides an important basis for the quantitative assessment of the defect size by infrared thermal imaging.

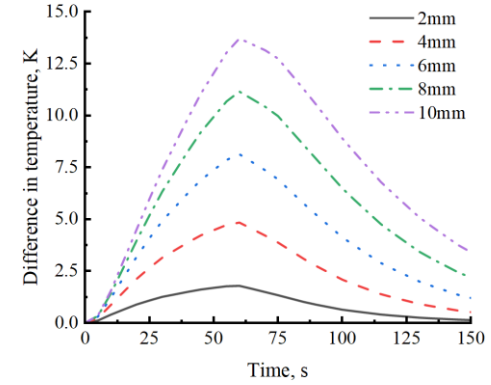

a

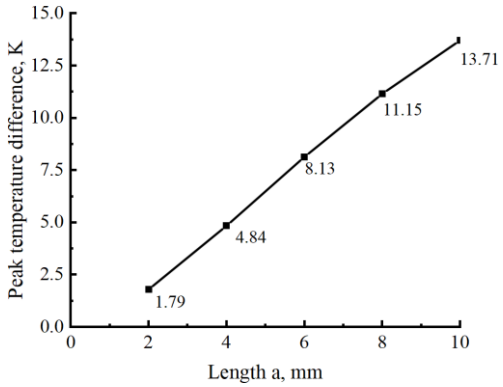

b

Fig. 8. Relationship between defect length and thermal response parameters: a – effect of defect length on thermal image temperature difference; b – relationship between defect length and peak thermal image temperature difference

3.2. Effect of defect thickness on heat transfer

Under the condition of controlling the defect length a = 6 mm and depth c = 2.5 mm, the influence of the defect thickness b (0.25 – 1.25 mm) on the thermal response characteristics was systematically investigated, and the experimental results of different defects are shown in Fig. 9, which shows that the distribution of the temperature field presents a typical 'crater' pattern. The temperature field distribution shows a typical 'crater' pattern, with a high-temperature zone formed in the centre of the defect and the temperature gradient decaying radially. A quadratic regression model of $\Delta T_{\text{-peak}}$ is established for the defect thickness$_{\text{-peak}}$ temperature difference, with $\Delta T_{\text{-peak}} = -3.11\, b^2 + 8.08\, b + 3.85$, substituting the thickness b showed that the model's predictions for $\Delta T_{\text{-peak}}$ deviated from the theoretical values by a maximum of 1.76 % and a minimum of 0.38 %. The slopes of the curves differ between the thicknesses of 0.25 – 0.75 mm and 0.75 – 1.25 mm, and the slope of the curve between the intervals of 0.25 and 0.75 mm is 5.03 K/mm, and that between 0.75 and 0.25 mm is 5.03 K/mm. K/mm, and the slope of 0.75 – 1.25 mm interval is 2.03 K/mm, when the thickness is $\leq$ 0.75 mm, the thermal resistance effect dominates and the temperature response is sensitive, and when the thickness is $\geq$ 0.75 mm, the thermal capacitance effect enhances and the growth rate decreases; this study quantitatively reveals the nonlinear relationship between the defect thickness and the thermal response, and the experimental data show that when the defect thickness exceeds 1.0 mm, the detection sensitivity will be decrease.

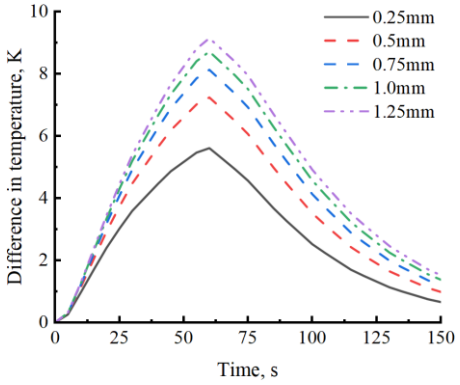

a

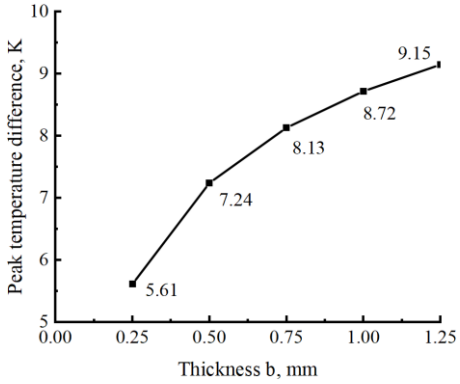

b

Fig. 9. Relationship between defect thickness and thermal response parameters: a – effect of defect thickness on thermal image temperature difference; b – relationship between defect thickness and peak thermal image temperature difference

3.3. Effect of defect depth on heat transfer

Under the experimental conditions of fixed defect length a = 3 mm and thickness b = 0.3 mm, the temperature response characteristics obtained by changing the defect depth c (0.5 – 4.5 mm) are shown in Fig. 10. Transient thermal response characteristics (Fig. 10 a), the rapid response stage 0 – 30 s, the slope of the temperature difference curve increases with every 1mm increase in depth; the decay stage > 60 s, the temperature difference shows an exponential decay characteristic, and the specimens with a shallower c < 2 mm depth decline at a faster rate, with a decay rate of -1.28 K/s.

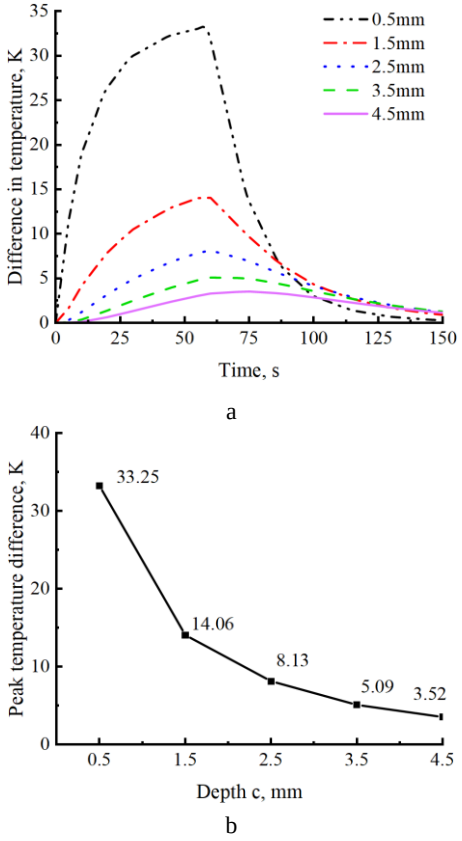

Fig. 10. Relationship between defect depth and thermal response parameters: a – effect of defect depth on thermal image temperature difference; b – relationship between defect depth and peak thermal image temperature difference

The curve crossing phenomenon occurs in 85 s – 100 s. For the depth of larger c ≥ 3 mm specimens, the decay rate is flat, -0.05 K/s ± 0.01, depth-peak relationship (Fig. 10 b), the establishment of the defect depth-$_{peak}$ temperature difference ΔT_{peak} quadratic regression model, $\Delta T_{peak} = 2.72\ c^2 - 20.46c + 41.49$, substituting the depth c showed that the model's predictions for ΔT_{peak} deviated from the theoretical values by a maximum of 37.13 % and a minimum of 1.42 %. Shallow defects (c < 2.5 mm): short heat diffusion paths, surface heat buildup effect significant; deep defects (c ≥ 2.5 mm), heat flow diffusion leads to signal attenuation appearing in the detection of the blind zone, the recommended excitation time is 40 – 70 s. The study quantitatively characterises the non-linear relationship between the depth of the defects and the thermal response, and the experimental data show that when the defect depth exceeds 3.5 mm, the infrared detection sensitivity will be significantly reduced, this finding provides an important basis for the development of detection standards for layered defects.

4. DEFECT PARAMETER ORTHOGONAL TEST

Limitation analysis and orthogonal experimental design based on univariate experiments: the limitations of the study illustrate that, although the independent relationship between each defect parameter (length a, thickness b and depth c) and the surface temperature difference ΔT was obtained through the aforementioned univariate control experiments, there are deficiencies, such as the inability to quantify the multi-parameter coupling effect, the difficulty in determining the significance ranking of the parameter effects, and the lack of parameter interaction analyses. To systematically study the multi-parameter synergistic effect, three parameters of delamination defects, length a, thickness b and depth c, were taken, and five levels were selected for each parameter to carry out orthogonal tests, and their factors and levels are shown in Table 2.

Table 2. Orthogonal test factors and levels

Orthogonal level	Factors		
	Length *a*, mm	Thickness *b*, mm	Depth *c*, mm
1	2	0.25	0.5
2	4	0.5	1.5
3	6	0.75	2.5
4	8	1	3.5
5	10	1.25	4.5

Continuing to follow the above external stimulus approach using the stimulus conditions and selected characteristics of the point, each experimental combination of three repetitions, through the polar analysis to determine the order of the factors primary and secondary, ANOVA to assess the significance of the factors, the orthogonal experimental design can be an effective solution to the limitations of single-factor research, while through 25 groups of experiments can be a comprehensive assessment of the parameter space of the three-factor five levels, significantly improving the efficiency of the study, the experimental results will provide key data to support the development of an infrared thermal imaging model that determines defect size. Taking the maximum temperature difference on the outer surface of the gas cylinder as the evaluation target, the results of the finite element analysis are shown in Table 3.

The FEA results of the table were analysed for significance and the ANOVA results for the maximum temperature difference on the outer surface of the gas cylinder were obtained as shown in Table 4.

Based on the results of the orthogonal experimental design analysis of variance in Table 4, the following conclusions can be drawn: In terms of the significance of parameter effects, defect depth contributes 53.7 % ($F = 13.61$, $p < 0.001$), indicating a highly significant influence; defect length contributes 19.2 % ($F = 4.882$, $p = 0.014$), indicating a significant influence; while defect thickness contributes only 6.5 % ($F = 2.035$, $p = 0.153$), indicating no significant influence.

Table 3. Finite element analysis results

Serial number	Length a, mm	Thickness b, mm	Depth c, mm	$\Delta T_{\text{-max}}/K$
1	2	0.25	0.5	5.77
2	2	0.5	2.5	1.58
3	2	0.75	4.5	0.78
4	2	1	1.5	3.50
5	2	1.25	3.5	1.36
6	4	0.25	4.5	1.52
7	4	0.5	1.5	7.60
8	4	0.75	3.5	3.05
9	4	1	0.5	22.02
10	4	1.25	2.5	5.54
11	6	0.25	3.5	3.64
12	6	0.5	0.5	27.92
13	6	0.75	2.5	8.17
14	6	1	4.5	3.72
15	6	1.25	1.5	16.29
16	8	0.25	2.5	7.52
17	8	0.5	4.5	4.53
18	8	0.75	1.5	19.55
19	8	1	3.5	7.60
20	8	1.25	0.5	54.80
21	10	0.25	1.5	14.42
22	10	0.5	3.5	7.97
23	10	0.75	0.5	53.55
24	10	1	2.5	14.74
25	10	1.25	4.5	6.93

Table 4. Results of significance analysis

Item	Defect size parameters			Error
	Length a, mm	Thickness b, mm	Depth c, mm	
DOF	4	4	4	12
MSE	259.404	108.14	723.124	53.132
F	4.882	2.035	13.61	
Significance	0.014	0.153	< 0.01	

The order of influence of the parameters is: defect depth (c) > defect length (a) > defect thickness (b). The study indicates that the depth of layered defects has a highly significant impact on the maximum temperature difference on the outer surface of the cylinder. This conclusion provides a theoretical basis for optimizing cylinder inspection protocols. It is recommended to prioritize depth parameter inspections, with inspection parameter settings focusing on area-type defect identification. Changes in thickness should be verified in conjunction with other inspection methods.

5. DISCUSSION

The superior performance of the external thermal excitation method – evidenced by a higher temperature contrast ($\Delta T_2'_{\text{max}}$ = 37.2 K) and a more practical detection time window (45 – 90 s) – can be attributed to fundamental heat transfer mechanisms. This approach generates a radial heat flux perpendicular to the defect plane, wherein the low thermal conductivity and thermal effusivity of the air-filled defects act as a pronounced thermal barrier. This results in localized heat accumulation and a distinct hot spot on the surface directly above the defect [14, 16]. In contrast, internal excitation employs convective heating, which tends to homogenize the temperature field of the inner liner prior to conduction through the composite wall. Consequently, this process inherently smears the thermal signal, leading to diminished contrast and a delayed appearance of the defect indication, as reflected in the smaller observed temperature difference (ΔT_{1_max} = 19.2 K) and a narrower detection window (35 – 60 s). These challenges in effectively quantifying internal thermal excitations, due to complex convective boundary conditions, have also been noted by Wang et al [13].

A quantitative relationship between defect parameters and the surface thermal response has been established, providing a crucial foundation for defect characterization. The near-linear correlation between defect length and the peak temperature difference ($\Delta T_{\text{-peak}} = 1.53\,a + 1.21$) confirms that larger defect areas impede a greater cross-section of heat flow, resulting in a stronger thermal signal. This trend is consistent with observations reported in studies on planar composite structures [18, 19]. In contrast, the nonlinear relationships for both defect thickness and depth highlight the complex interplay of thermal resistance and thermal capacitance. The established quadratic model for thickness ($\Delta T_{\text{-peak}} = -3.11\,b^2 + 8.08\,b + 3.85$) reveals that beyond a specific threshold (~0.75 mm), an increase in the air gap volume enhances its heat storage capacity, which slows the surface temperature rise and diminishes the peak contrast – an effect often overlooked in simpler models. This nuance underscores the critical importance of the multi-parameter analysis conducted in this work.

Critically, the orthogonal experimental analysis reveals that defect depth is the most influential parameter, contributing 53.7 % to the observed variation. This finding both supports and refines previous research, as the strong dependence of thermal contrast on defect depth is a widely established principle in transient thermography. For instance, Ekanayake et al. [17] demonstrated the influence of depth on contact resistance in phase-locked thermal imaging, while Kalyanavalli et al. [21] established a relationship between defect depth and peak time in long-pulse thermography. Our study reinforces these findings, confirming depth as the primary determinant of thermal contrast. Conversely, the comparatively minor contribution of defect thickness 6.5 % suggests that the presence of an air gap itself creates the dominant thermal resistance, while its precise dimension within a typical range is a secondary factor. This insight is of particular practical value for non-destructive testing: it indicates that while accurate depth characterization is essential, estimating the precise thickness of a delamination via thermography alone remains challenging and typically requires supplemental techniques [12, 15].

The practical significance of this research is demonstrated through a validated and optimized inspection protocol for Type III cylinders. It is recommended to utilize an external excitation detection window centered around 60 – 75 s, thereby enhancing inspection reliability and efficiency. Furthermore, the established significance ranking of parameters (depth > length > thickness) provides a critical prioritization framework for defect assessment algorithms. This framework can directly inform the development of automated inspection systems that utilize machine learning, as explored by Daghigh and Naraghi [18],

potentially significantly improving their sizing and characterization accuracy.

6. CONCLUSIONS

1. This study systematically compared internal and external thermal excitation methods for detecting delamination defects in Type III composite cylinders. Results demonstrated the clear superiority of the external excitation approach, which produced a significantly higher temperature contrast (up to 37.2 K) and a wider, more practical detection time window (45 – 90 s). These findings thus provide a definitive theoretical and empirical basis for selecting excitation methods in industrial non-destructive testing settings.
2. This study developed quantitative models describing the influence of key defect parameters (length, thickness, depth) on the surface thermal response. Specifically, the established linear relationship with defect length and the nonlinear relationships with both thickness and depth provide a predictive framework for defect characterization, representing a significant advancement over qualitative assessments.
3. Critically, the orthogonal experimental design and analysis of variance enabled the quantification of the relative significance of each defect parameter for this specific structure. The results establish that defect depth is the single most influential parameter (53.7 % contribution), followed by length and then thickness, thereby offering a novel, quantitative hierarchy for defect assessment. This insight shifts the focus of quantitative analysis toward depth estimation, refining the theoretical understanding of heat flow around subsurface defects in composite materials.
4. Overall, these findings effectively bridge the gap between fundamental research in thermal imaging and specialized industrial applications. The proposed optimized inspection protocol, underpinned by the parameter significance analysis, provides a direct and valuable contribution to the field. This work enhances the reliability, efficiency, and interpretability of non-destructive evaluation for composite pressure vessels, ultimately leading to significant improvements in their operational safety and structural integrity.

Acknowledgments

This work was supported by the Central Guided Local Special Project (2024ZYD0125) and the Shaanxi Provincial Key R&D Program (2024CY-GJHX-05) and the Key Laboratory of Manufacturing and Application of Intelligent Well Control for Oil and Gas Production and Transportation of Luzhou Project (2025LZOGB-10).

REFERENCES

1. **Koutsawa, Y., Bouhala, L.** Uncertainty Analysis in the Sesign of Type-IV Composite Pressure Vessels for Hydrogen Storage *Composites Part C: Open Access* 16 2025: pp. 100544. https://doi.org/10.1016/j.jcomc.2024.100544
2. **Meemary, B., Vasiukov, D., Deléglise-Lagardère, M., Chaki, S.** Sensors Integration for Structural Health Monitoring in Composite Pressure Vessels: A Review *Composite Structures* 351 2025: pp. 118546. https://doi.org/10.1016/j.compstruct.2024.118546
3. **Agne, L.L., Almeida, Jr.J.H.S., Amico, S.C., Tonatto, M.L.** Impact of Stacking Sequence on Burst Pressure in Glass/Epoxy Type IV Composite Overwrapped Pressure Vessels for CNG Storage *International Journal of Pressure Vessels and Piping* 212 2024: pp. 105315. https://doi.org/10.1016/j.ijpvp.2024.105315
4. **Zhou, W., Wang, J., Pan, Z.B., Liu, J., Ma, L.H., Zhou, J.Y., Su, Y.F.** Review on Optimization Design, Failure Analysis and Non-Destructive Testing of Composite Hydrogen Storage Vessel *International Journal of Hydrogen Energy* 47 (91) 2022: pp. 38862 – 38883. https://doi.org/10.1016/j.ijhydene.2022.09.028
5. **Weisberg, A.H., Aceves, S.M., Espinosa-Loza, F., Ledesma-Orozco, E., Myers, B., Spencer, B.** Cold Hydrogen Delivery in Glass Fiber Composite Pressure Vessels: Analysis, Manufacture and Testing *International Journal of Hydrogen Energy* 38 (22) 2013: pp. 9271 – 9284. https://doi.org/10.1016/j.ijhydene.2013.05.068
6. **Syed, Z.A.H., Che, J.L., Chang, S.H.** Design of a Type-III Hydrogen Pressure Vessel with an Elliptical Dome for Stress Reduction in the Composite Layer *International Journal of Hydrogen Energy* 103 2025: pp. 937 – 950. https://doi.org/10.1016/j.ijhydene.2025.01.215
7. **Eko, A.J., Epaarachchi, J., Jewewantha, J., Zeng, X.** A Review of Type IV Composite Overwrapped Pressure Vessels *International Journal of Hydrogen Energy* 109 2025: pp. 551 – 573. https://doi.org/10.1016/j.ijhydene.2025.02.108
8. **Wang, Q., Qin, H., Jia, L., Li, Z., Zhang, G., Li, Y., Liu, Y.** Failure Prediction and Optimization for Composite Pressure Vessel Combining FEM Simulation and Machine Learning Approach *Composite Structures* 337 2024: pp. 118099. https://doi.org/10.1016/j.compstruct.2024.118099
9. **Ge, L., Zhao, J., Li, H., Dong, J., Geng, H., Zu, L., Yang, X.** A Three-Dimensional Progressive Failure Analysis of Filament-Wound Composite Pressure Vessels with Void Defects *Thin-Walled Structures* 199 2024: pp. 111858. https://doi.org/10.1016/j.tws.2024.111858
10. **Hu, C., Fu, X., Yuan, Y., Xiao, B., Sun, M., Yang, B.** A Novel Damage Localization Technique for Type III Composite Pressure Vessels Based on Guided Wave Mode-Matching Method *Composite Structures* 346 2024: pp. 118414. https://doi.org/10.1016/j.compstruct.2024.118414
11. **Tao, N., Groves, R.M., Anisimov, A.G.** Shearography Pair Method for Reliable Non-Destructive Inspection of Millimeter and Submillimeter Defects in Fiber-Reinforced Composites *Measurement* 2025: pp. 117980. https://doi.org/10.1016/j.measurement.2025.117980
12. **Ma, L., Liu, C., Han, J., Wen, A., Liu, B., Zheng, J.** Delamination Defects in Composite Hydrogen Storage Cylinders: CT Scanning and Shearography Measurement *International Journal of Hydrogen Energy* 97 2025: pp. 140 – 149. https://doi.org/10.1016/j.ijhydene.2024.11.447
13. **Wang, G., Mao, Z., Yu, H., Chen, H., Sun, S.** Fuzzy Estimation for Transient Distribution of Internal Thermal Excitation in Composite Overwrapped Pressure Vessel *Applied Thermal Engineering* 203 2022: pp. 117866. https://doi.org/10.1016/j.applthermaleng.2021.117866

14. **Aramburu, A.B., da Cruz, J.A., da Silva, A.A.X., Acosta, A.P., Minillo, L.Q., de Avila Delucis, R.** Non-Destructive Testing Techniques for Pressure Vessels Manufactured with Polymer Composite Materials: A Systematic Review *Measurement* 2025: pp. 116729. https://doi.org/10.1016/j.measurement.2025.116729
15. **de Bortoli, T.J., Barros, V.T., Albertazzi, A.** Classification and Sizing of Circular Defects in Composite Coated Metal Plates Using Thermography and Neural Networks *Measurement* 249 2025: pp. 116815. https://doi.org/10.1016/j.measurement.2025.116815
16. **Al-Athel, K.S., Alhasan, M.M., Alomari, A.S., Arif, A.F.M.** Damage Characterization of Embedded Defects in Composites Using a Hybrid Thermography, Computational, and Artificial Neural Networks Approach *Heliyon* 8 (8) 2022: pp. e10063. https://doi.org/10.1016/j.heliyon.2022.e10063
17. **Ekanayake, S., Gurram, S., Schmitt, R.H.** Depth Determination of Defects in CFRP-Structures Using Lock-in Thermography *Composites Part B: Engineering* 147 2018: pp. 128 – 134. https://doi.org/10.1016/j.compositesb.2018.04.032
18. **Daghigh, V., Naraghi, M.** Machine Learning-Based Defect Characterization in Anisotropic Materials with IR-Thermography Synthetic Data *Composites Science and Technology* 233 2023: pp. 109882. https://doi.org/10.1016/j.compscitech.2022.109882
19. **Grosso, M., de Araújo Soares, I., Lopez, J.E., Soares, S. D., Rebello, J.M., Pereira, G.R.** Study on the Limit Detection of Defects by Pulsed Thermography in Adhesive Composite Joints Through Computational Simulation *Composites Part B: Engineering* 168 2019: pp. 589 – 596. https://doi.org/10.1016/j.compositesb.2019.03.083
20. **Sirikham, A., Zhao, Y., Liu, H., Xu, Y., Williams, S., Mehnen, J.** Three-Dimensional Subsurface Defect Shape Reconstruction and Visualisation by Pulsed Thermography *Infrared Physics & Technology* 104 2020: pp. 103151. https://doi.org/10.1016/j.infrared.2019.103151
21. **Kalyanavalli, V., Ramadhas, T.A., Sastikumar, D.** Long Pulse Thermography Investigations of Basalt Fiber Reinforced Composite *NDT & E International* 100 2018: pp. 84 – 91. https://doi.org/10.1016/j.ndteint.2018.08.007
22. **Zhang, J., Jiang, W., Zhu, P., Zheng, T.** Sealing Performance and Mechanical Response of Mud Pump Piston *Petroleum* 9 (1) 2023: pp. 101 – 107. https://doi.org/10.1016/j.petlm.2021.12.004
23. **Zhang, J., Yu, C.Q.** Simulation Study on Defect Detection of Carbon Fiber Wrapped Hydrogen Storage Cylinders Based on Infrared Thermal Imaging *Journal of Safety Science and Technology* 20 (12) 2024: pp. 82 – 89. 10.11731/j.issn.1673-193x.2024.12.011